J Appl Electrochem (2010) 40:639–651
DOI 10.1007/s10800-009-0039-4

ORIGINAL PAPER

XPS and EIS studies of sputtered Al–Ce films formed on AA6061 aluminum alloy in 3.5% NaCl solution

M. A. Domínguez-Crespo · A. M. Torres-Huerta · S. E. Rodil · S. B. Brachetti-Sibaja · W. de la Cruz · A. Flores-Vela

Received: 25 May 2009 / Accepted: 23 November 2009 / Published online: 9 December 2009

Abstract X-ray photoelectron spectroscopy (XPS) was used to analyze the composition of films at different deposition parameters of sputtered Al-Ce coatings on AA6061 aluminum alloys. By means of electrochemical impedance spectroscopy (EIS) measurements, the protective character of these coatings was studied for 21 days of exposure in a 3.5 wt% NaCl solution and an attempt was made to establish the relationship between film thickness and chemical composition (Al/Ce, Ce^3/Ce^{4+} ratios) of the surface before and after the electrochemical characterization. XPS studies revealed the presence of the Al^o, Al_2O_3, CeO_2 and Ce_2O_3 compounds, confirming that the sputtered Al-Ce films were deposited in the metallic form and thereafter were superficially oxidized under ambient conditions. The Al–Ce bonds were overlapped with the signal of cerium oxides. The transport phenomena in the oxide film or controlled diffusion process are strongly dependent on the deposition parameters and exposure time in the aggressive medium. It was also found that in the deposited samples at $p_4P_{200}t_{300}$, the film was still present after 21 days of exposure, although with visible cracks and erosion areas; however, the Ce^3/Ce^{4+} ratio almost remained constant before and after the electrochemical characterization, which explained the barrier properties of these samples as compared with others at different deposition parameters.

Keywords AA6061 · Magnetron sputtering · Coatings · Corrosion properties · Al–Ce films

M. A. Domínguez-Crespo (✉) · A. M. Torres-Huerta · A. Flores-Vela
CICATA-Altamira, IPN, km 14.5, Carretera Tampico-Puerto Industrial Altamira, C.P. 89600 Altamira, Tamps, Mexico
e-mail: mdominguezc@ipn.mx; adcrespo2000@yahoo.com.mx

S. B. Brachetti-Sibaja
Alumna PTA-CICATA-Altamira IPN, km 14.5, Carretera Tampico-Puerto Industrial Altamira, Tamps, Mexico

S. E. Rodil
IIM-UNAM, Circuito Exterior s/n, Ciudad Universitaria, Del. Coyoacán, C.P. 04510 México, D.F., Mexico

W. de la Cruz
Centro de Nanociencias y Nanotecnología, UNAM, A. Postal 2681, 22800 Ensenada, B.C., Mexico

1 Introduction

Aluminum and its alloys represent an important category of materials due to their high technological value and wide range of industrial applications, especially in aerospace and household industries. The use of these materials in lightweight installations is widespread. The resistance of aluminum and its alloys to corrosion is known to be due to the formation of a surface film comprised primarily of alumina (Al_2O_3) [1, 2], an electrically insulating material with a band gap in excess of 3 eV [3]. However, the enrichment of the alloy elements, such as oxides, into the surface film or the addition of coatings to form a new layer has been observed to enhance the properties against corrosion of the aluminum-based structures [4–6]. Recent patents cover a wide variety of new coating formulations [7–10]. One of the most promising systems is based on rare earth elements. In a series of papers [11, 12], several researchers demonstrated that treatments with aqueous solutions of rare earth salts (cerium, lanthanum, neodymium and yttrium) effectively inhibited the corrosion of aluminum alloys. In a recent published work, we investigated the relationship between the microstructure of sputtered Al–Ce thin films as a new alternative to improve the corrosion resistance of

AA6061 aluminum alloys by RF magnetron sputtering [13]. This study revealed that the selected parameters (power and pressure) have a high influence on the composition of the film probably as a consequence of the significant difference in the sputtering yield of Ce and Al, depending on the operating conditions. During this process, films with very fine nanocrystals, "metallic glasses" or amorphous films can be obtained as a consequence of the polymorphic transitions of cerium [14]. This metallic glass films were composed of small crystallites of $CeAlO_3$, Al_4Ce, Al_3Ce combined with cerium oxides; this composition seems to have significant influence on the preliminary corrosion behavior, inhibiting the cathodic and anodic reactions and increasing impedance values after 1 day of continuous immersion in the aggressive medium. Due to the fact that corrosion in aluminum alloys is a very complex process that can be affected by various factors such as the type of aggressive ion and its concentration, the pH of the media, temperature or structural characteristics of the oxide passive film [1, 15–23], an understanding of the characteristics of the proposed films can be a crucial step towards the formulation of effective mitigation strategies. Given that electrochemical impedance spectroscopy (EIS) and XPS are two techniques that provide information on the surface of the material [24], this research work used them to interpret the electrochemical behavior of sputtered Al–Ce coatings during 21 days of exposure in a 3.5 wt% NaCl solution and correlated it with the nature and composition of the deposited films before and after the corrosion product layer was formed on the surface under the experimental conditions.

2 Experimental procedure

2.1 Film deposition

In this work, aluminum-based coatings deposited by a commercial DC magnetron sputtering apparatus from a multicomponent target consisting of Al (99.95% purity, diameter of 100 mm and thickness of 3 mm) and eight Ce pieces (99.5% purity, 15 × 5 × 1 mm) attached to the Al target race track were used to analyze the nature and composition of the films before and after the electrochemical tests. Two sets of experiments were carried out. In the first set, the pressure was increased from 6.67×10^{-1} to 4 Pa at 200 W ($p_{0.667}P_{200}t_{300}$, $p_{1.333}P_{200}t_{300}$, $p_4P_{200}t_{300}$); and in the second set, power was varied from 40 to 280 W at a constant pressure of 4 Pa ($p_4P_{280}t_{300}$, $p_4P_{120}t_{300}$and $p_4P_{40}t_{300}$). The synthesis of sputtered Al-Ce coatings and information of the magnetron sputtering apparatus have been described in detail elsewhere [13].

2.2 Surface analysis

XPS analyses were performed on coated samples using an AES-XPS PHI-548 spectrometer after exciting the samples by an unmonochromatized Al K_α line at 1486.6 eV. The working pressure was $<1 \times 10^{-10}$ Pa. The energy scale was calibrated using thick films of copper with line at 932.67 eV for Cu $2p_{3/2}$. Survey scans were obtained in the 1205-(-10) eV energy interval at 1.0 eV per step, pass energy of 100 eV. Additionally, the high-resolution XPS scans were completed at 0.2 eV energy steps and pass energy of 50 eV (constant pass energy mode). The measured full-width half-maximum (FWHM) for the Cu $2p_{3/2}$ line in metallic state with these settings is 1.6 eV. These detailed scans were recorded for the Al2p, $Ce3d_{5/2}$, C1s and O1s for the coated samples. Also, detailed scans for the Al2p, $Ce3d_{5/2}$, C1s, O1s, $Cl2p_3$ and Na1s were verified after electrochemical evaluation. The analyzed area of the XPS measurements was 800 μm^2.

The coating surface of all the samples was evaluated using a SEM/EDS (JEOL JSM-5600LV), before and after the electrochemical tests.

2.3 EIS measurements

EIS was used to evaluate the changes in the barrier properties of the Al–Ce films in a 3.5 wt% NaCl solution for 21 days. An electrochemical cell consisting of an acrylic rectangular box (60 × 80 × 100 mm) was used during the experimental tests. The cell was formed by a saturated calomel reference electrode (SCE), a graphite bar counter electrode, and the working electrode was comprised by the surface (1.23 cm^2) of the coated samples delimited by the inner wall of the cell. Twelve hours were allowed to pass in order to the corrosion potential (E_{corr}) to stabilize. A Gamry reference 600 potentiostat/galvanostat with a frequency response analyzer ZRA was used in the 100 kHz to 0.01 Hz frequency range spaced logarithmically (ten frequency points per decade). The width of the sinusoidal voltage signal applied to the system was 10 mV rms (root-mean-square). The results were fitted with the Echem Analyst 5.5 software.

3 Results and discussion

3.1 Composition and related spectra of the sputtered Al–Ce coatings on AA6061 aluminum alloy

Previously discussed results have shown that the deposition parameters exert a strong influence on the morphology, thickness and Al/Ce ratio [13]. Due to the fact that the electrochemical performance depends on the cerium

Table 1 Thickness, Al/Ce ratio, Ce^{3+}/Ce^{4+} ratios obtained in the sputtered Al-Ce films, according to the deposition parameters

Deposition parameters	Thickness (nm)	Al/Ce ratio	Ce^{3+}/Ce^{4+} ratios before EIS measurements	Ce^{3+}/Ce^{4+} ratios after EIS measurements
$p_4P_{200}t_{300}$	1214.5	0.6028	1.088	1.080
$p_4P_{280}t_{300}$	1171.7	0.4729	1.511	No detected
$p_4P_{120}t_{300}$	524.1	0.1761	1.462	No detected
$p_4P_{40}t_{300}$	102.2	0.0101	1.440	No detected
$p_{1.333}P_{200}t_{300}$	511.1	0.1606	2.741	No detected
$p_{0.667}P_{200}t_{300}$	262.4	0.0683	1.316	No detected

quantity and thickness, Table 1 displays the experimental results focused on thickness and Al/Ce ratio.

The low-resolution XPS spectra of the Al–Ce coatings at different sputter deposition parameters (pressure and power) on AA6061 aluminum alloys are shown in Fig. 1. The survey spectrum recorded for the samples reveals that besides Al and Ce, significant amounts of O were present in the outer layer of the coatings. The presence of partial O has been formerly attributed to the reactivity of Al and Ce under ambient conditions [13, 25]. There is also a small amount of C on the surface of the thin films; however, this may be the adsorbed C from the air. In fact, it is well known that the carbon peak almost always appears in any XPS analysis, although some of the samples contain no carbon at all [25, 26]. The high-resolution Al2p, $Ce3d_{5/2}$ and O1s core level spectra are reported in Figs. 2, 3, and 4 for the different deposition parameters. The presence of aluminum in the form of Al^{3+} and in metallic state (Al^{o}) was detected by the Al2p peak, which shows in some cases two components at binding energies of 74.4 eV, which may be associated with the presence of aluminum in the Al^{3+} form, and a less intense component at 71.2 eV, which is correlated with the metallic state form (Fig. 2), while in another spectra, the Al_2O_3/Al^{o} signals were overlapped and it was hard to separate the signals. The presence of Al^{o} in the coatings confirms that the Al–Ce films were deposited

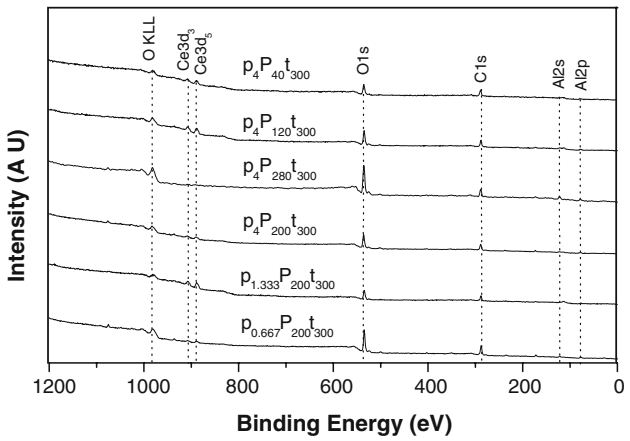

Fig. 1 XPS survey spectra of the Al–Ce coatings at different deposition parameters on AA6061 aluminum alloys

in the metallic form and later their surface oxidation under ambient conditions occurred, which had been previously suggested [13]. High-resolution spectra of $Ce3d_{5/2}$ and $Ce3d_{3/2}$ are shown in Fig. 3. In all the analyzed sputtered coatings, cerium was present in the Ce^{4+} and Ce^{3+} states. The Ce3d spectrum is composed of two groups of spin–orbit splitting couple peaks. According to the spectrum, the peaks at 882.3, 900.7 and 907.5 eV were considered to belong to Ce^{4+}, while the couples at 885.9 and 904.1 eV were due to Ce^{3+} [27–29]; although these peaks can be overlapping with the Ce–Al and Ce metallic bonds that are reported at 883.50 and 883.90 eV, respectively. The μ''' peak, which arose from a transition from the $4f^{o}$ initial state to the $4f^{o}$ final state, which is frequently considered as a confirmation of the presence of Ce^{4+}, was missing in the XPS spectra; however, the other peaks associated with tetravalent cerium are clearly identified in the Ce3d signals and can be used to determinate the Ce^{3+}/Ce^{4+} ratio forming the film [30]. All inner Ce3d spectra had almost identical peak structures except for the quite different intensities. The Ce^{3+}/Ce^{4+} ratio forming the film is shown in Table 1. According to this data, Ce^{3+} was the dominant oxidation state of cerium for most of the sputtered Al–Ce in the films, although an important amount of Ce^{4+} can also be observed.

The O1s spectra shown in Fig. 4 are composed of two peaks at 529.5 and 531.5 eV, which may be due to oxygen in Ce–O and Al–O bonds, respectively. By considering the spectra of Ce, Al, O, and the results discussed above, it was proposed that the sputtered AlCe films were mainly composed on the surface by a combination of Ce_2O_3, CeO_2, and Al_2O_3, although it was hard to establish the presence of intermetallic compounds such as $CeAlO_3$, Al_4Ce, Al_3Ce, which must appear around 883.50 eV, but their presence cannot be discarded. It has been previously reported that the sputtered Al–Ce layer on this alloy varies from an approximately $\sim$300 nm to 1.3 μm thick layer depending on both the sputtering Ce yield in comparison to Al and deposition parameters [31]; the XPS analysis confirmed that the films were predominantly composed of a large amount of amorphous Al_2O_3 with small crystals of Ce_2O_3, CeO_2, $CeAlO_3$, Al_4Ce or Al_3Ce promoting a metallic glassy form, as it was previously suggested [13].

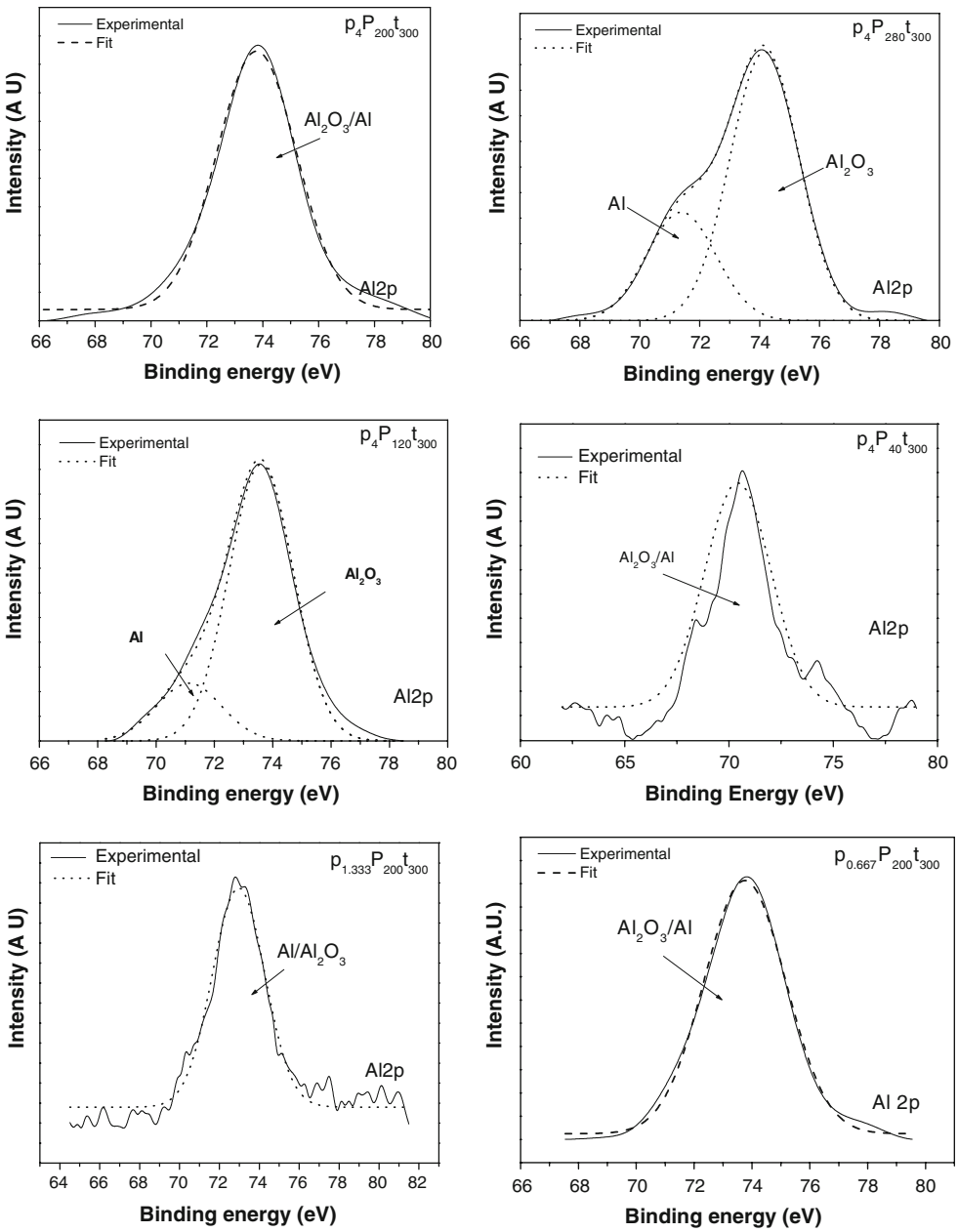

Fig. 2 High-resolution Al2p XPS spectra obtained on the surface of sputtered Al–Ce films formed on AA6061 aluminum alloy at different deposition parameters

3.2 EIS characterization

The use of EIS to investigate the corrosion behavior of coated metals is very popular, and it has been widely used to characterize Al surfaces coated with the traditional chromate-based coatings [32–35]. In fact, EIS is a quantitative tool to assess the evolution of the corrosion protection afforded by coatings or conversion layers [36]; however, as far as we know, works investigating the corrosion resistance of sputtered Al–Ce on aluminum alloys have not been published yet.

The evolution of the Nyquist diagrams for the sputtered samples obtained after 0, 5, 11, 16 and 21 days of immersion in a 3.5 wt% sodium chloride solution with 10 mV perturbation amplitude against their respective open circuit potentials (OCPs) are presented in Fig. 5. As illustrated in this figure, the as-deposited films and bare aluminum show a similar shape, but are considerably different in their sizes. During the time of exposure, all the experimental plots displayed a depressed semicircular shape in the complex impedance plane with the center under the real axis, which is a typical behavior of solid metal electrodes that show frequency dispersion in the impedance data [37, 38]. The samples also showed, in all the cases, a tail in the low-frequency range. Different authors have attributed these low-frequency features to transport phenomena in the oxide film or diffusion controlled processes [39, 40]. In our experiments, it has been noted that this feature is strongly

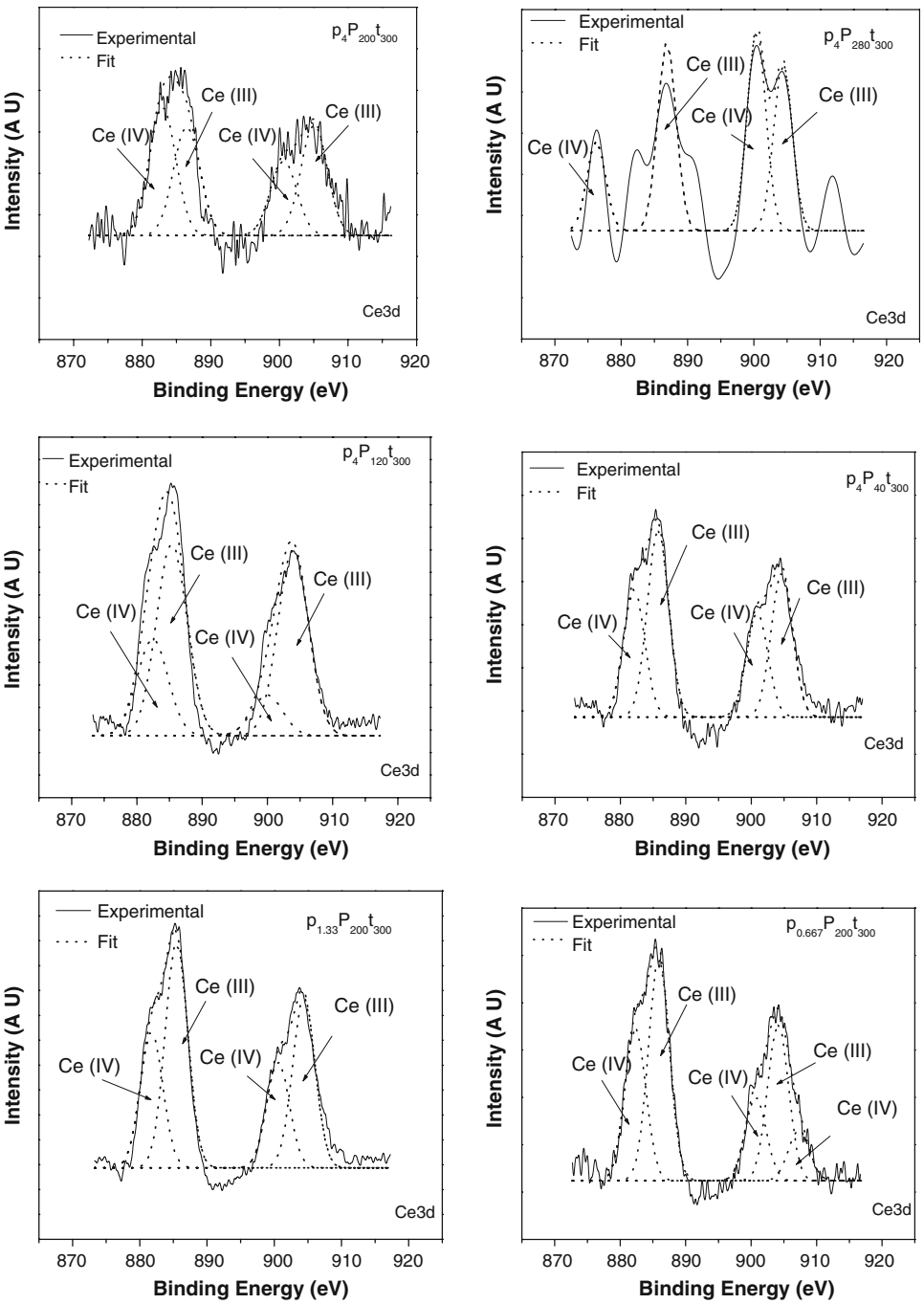

Fig. 3 High-resolution Ce3d XPS spectra obtained on the surface of sputtered Al–Ce films formed on AA6061 aluminum alloy at different deposition parameters

dependent on the deposition parameters and exposure time in the aggressive medium, i.e. as the immersion time is increased; the tail at low frequencies is also increased. Then, the intermediate frequency arc can be assimilated to a semicircle whose diameter defines an overall polarization resistance (R_p), which is the sum of partial resistances ($R_{coat} + R_{ct}$; coating resistance + charge transfer resistance) and the value of the capacitances (C_{coat}; capacitance of the coating and C_{dl}; capacitance of the double layer). Therefore, the EIS data were fitted by using the equivalent circuits shown in Fig. 6 [31], $R_s(C_{dl}\ [R_{ct}\ W])$ and $R_s(CPE_{film}[R_{film}\ (C_{dl}\ W)])$ for bare steel and coated samples, respectively. In specific, for the sputtered samples instantaneously immersed (0 day), the Nyquist plots exhibit an enhancement in the total resistance value in comparison with the bare AA6061 aluminum alloy (11,256 Ω cm^2). This trend is more evident by varying the power and fixing the pressure at 4 Pa. The total resistance values increased as power was increased to 200 W (278,276 Ω cm^2), and after this value (280 W), it began to decrease (122,256 Ω cm^2). The reduction in the total resistance values can be correlated with the deposition rate which in this case

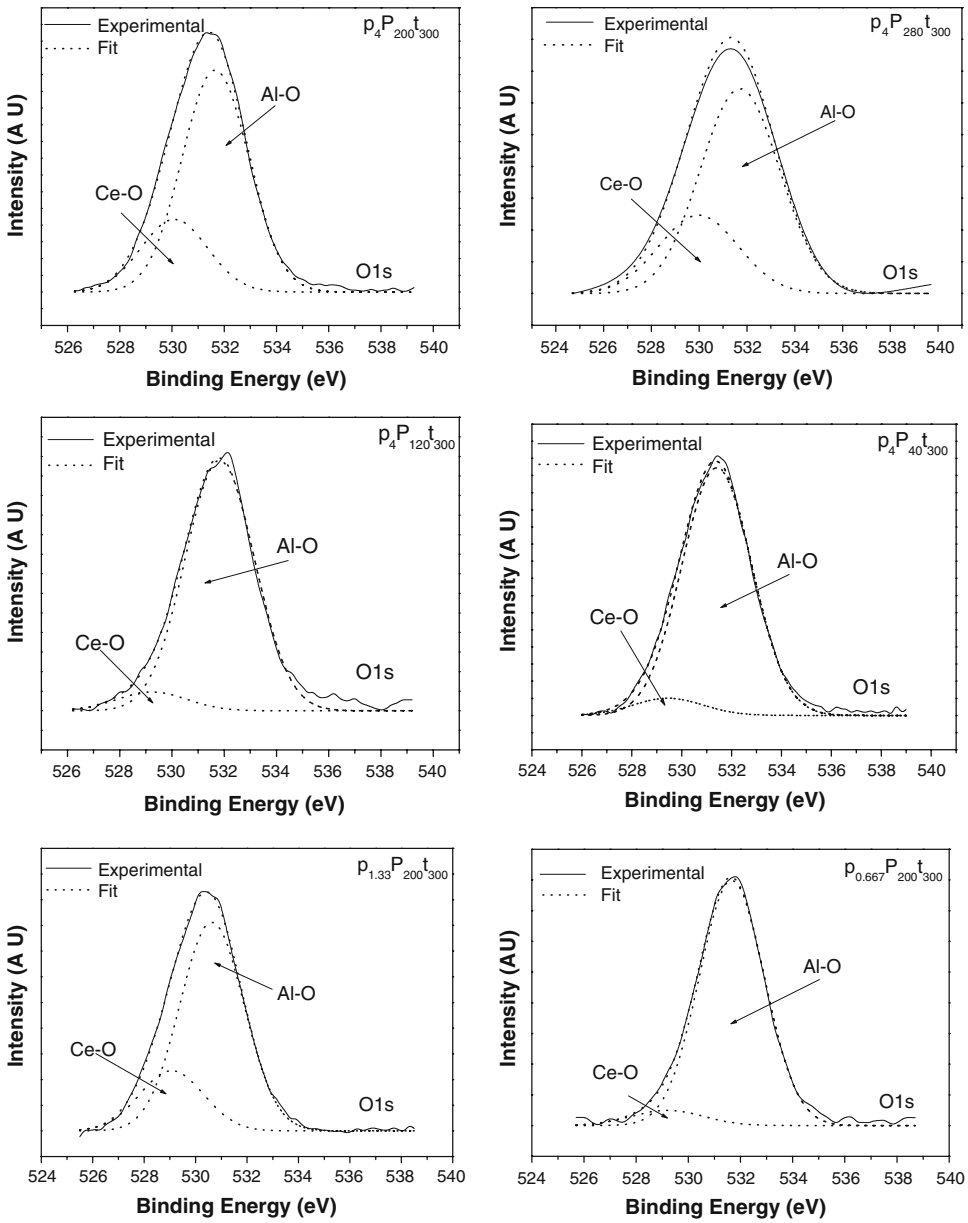

Fig. 4 High-resolution O1s XPS spectra obtained on the surface of sputtered Al–Ce films formed on AA6061 aluminum alloy at different deposition parameters

decreased from 4.04 to 3.90 nms^{-1}, probably by gas rarefication due to a higher amount of reactive cerium atoms in the plasma and the sputter yield of Al and Ce or both [13]. At this time, the evaluated coatings displayed different protection orders depending upon the balance between the deposition parameters, composition and thickness of the film. It is well known that for aluminum alloys [41], corrosion is a combination of at least two electrochemical reactions involving anodic areas where the metal dissolution occurs:

$$Al \rightarrow Al^{3+} + 3e^{-} \quad (1)$$

Whereas in the cathodic areas, reactions such as the reduction of oxygen can take place:

$$O_2 + 2H_2O + 4e^{-} \rightarrow 4OH^{-} \quad (2)$$

Then, all the deposited films inhibited both reactions, although with quite different corrosion properties. The order of the achieved protection at this immersion time was as follows: $p_4P_{200}t_{300} > p_4P_{280}t_{300} > p_4P_{120}t_{300} > p_{0.667}P_{200}t_{300} > p_{1.333}P_{200}t_{300} > p_4P_{40}t_{300}$ > bare aluminum with a polarization resistance of 278,276, 122,256, 99,422, 64,415, 16,790, 15,776 and 11,693 $\Omega\ cm^2$, respectively. As it can be seen from this figure, for exposure times of 5 and 11 days, the semicircle radius drastically decreases for all the samples, even for samples at $p_4P_{200}t_{300}$ (48,338 $\Omega\ cm^2$). It is clear that also at low frequencies, the tail is higher, indicating a linear variation of the impedance, which suggests that the diffusive controlled process becomes more important, maybe because of the evolution of the corrosion process. At this period of time, it is hard to identify a trend

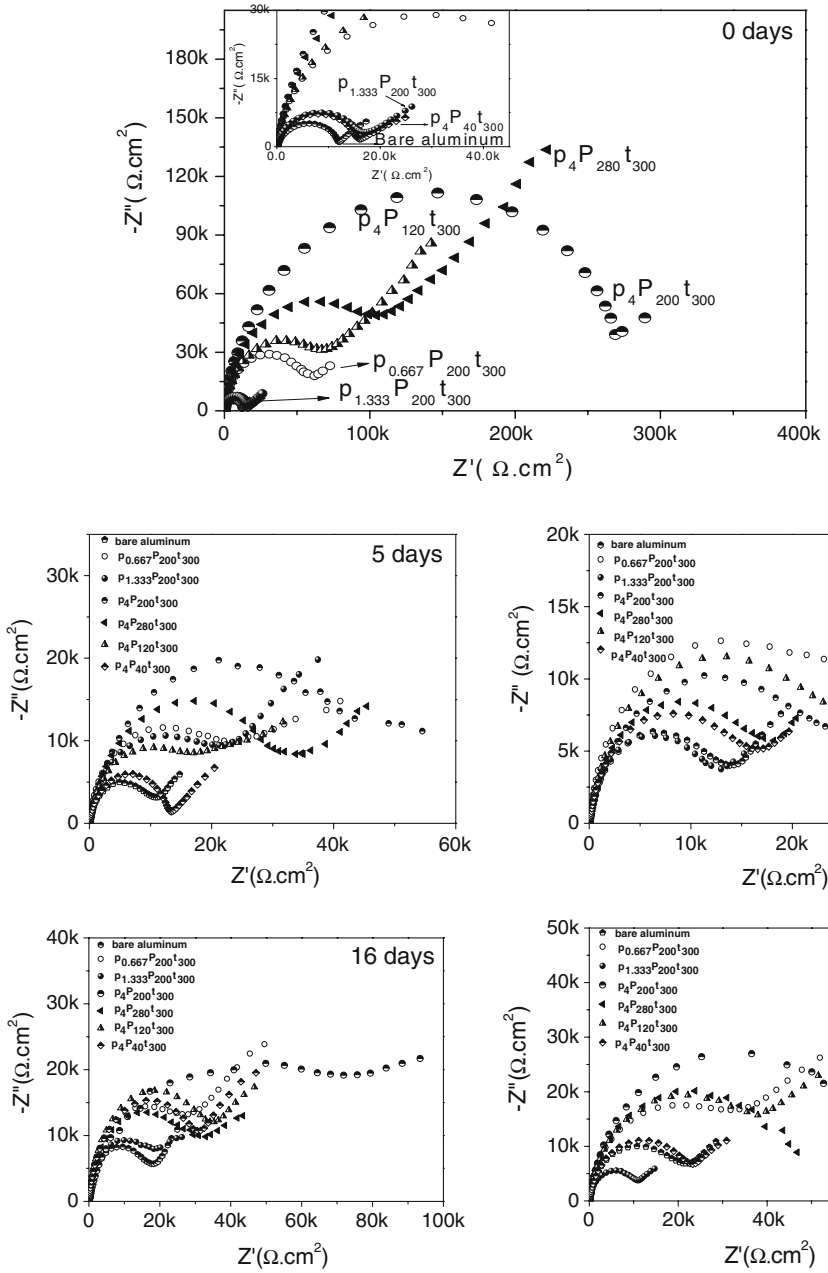

Fig. 5 Variation in Nyquist diagrams with exposure time in the aggressive media on sputtered samples and bare aluminum

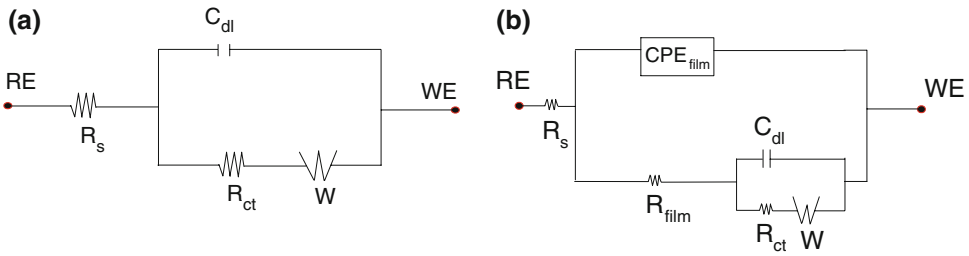

Fig. 6 Equivalent circuit of **a** bare aluminum and **b** coated specimens after 0, 1, 5, 11, 16 and 21 days of continuous immersion

in the properties against corrosion of the evaluated samples.

The important increase in the specimens at 16 days of continuous immersion (even in the aluminum) reflects the information of the corrosion process occurring on the substrate surface; i.e. this increase in the sputtered Al–Ce films suggests the interaction of cerium and alumina to form a new barrier, mainly hydrated oxides that prevent

solution ion penetration. It has been found that this barrier layer in aluminum is formed by a mixed Al–Ce oxy-hydroxide, where cerium cation can act as a substitutional cation for Al^{3+} ions within the alumina pattern [42, 43], and thus forms a protective layer that leads to increase the total resistance. As for the bare aluminum, the formation of alumina and aluminum hydroxide acts as a barrier that delays the penetration of the electrolyte [41]. Finally, at 21 days, the EIS plots show that the sputtered Al–Ce films at $p_{1.333}P_{200}t_{300}$ and $p_4P_{40}t_{300}$ have entirely lost their anti-corrosive properties, displaying similar or lower resistances (26,432 and 12,238 Ω cm^2) than those observed for the bare aluminum (24,474 Ω cm^2); and at the same time, pitting can be observed on the surface of the sample (it can even be seen with the naked eyes). This indicates that the new impedance of these samples reflects the information of the aluminium alloy, where the corrosion medium has already reached or permeated into the whole surface. On the other hand, for the specimens at $p_{0.667}P_{200}t_{300}$, $p_4P_{280}t_{300}$, and $p_4P_{120}t_{300}$, a slightly increase in the total impedance ($\sim$48 KΩ cm^2) can be observed, which is attributed to the cerium compounds still present on the substrate surface forming a protective barrier. As a final point, the Al–Ce films at $p_4P_{200}t_{300}$ showed the best electrochemical performance of the evaluated samples (67,059 Ω cm^2), even though the polarization resistance diminished in the range of 16 to 21 days of exposure. In addition, no severe damage was observed in the coated samples after this immersion time.

Figure 7 shows the evolution of the values of total polarization resistance with increasing exposure time (from 0 to 21 days) in the aggressive medium. Taking the bare aluminum as reference, in general (except for the samples at $p_{1.333}P_{200}t_{300}$), the Al–Ce sputtered films tend initially to diminish the impedance value with the immersion time and after 11 days, when some hydrated oxides are well-formed, the value of R_p associated with the semicircle increases; with regards to the importance of this effect, it is observed that 11 days of exposure are necessary to reach a steady state in the impedance values for some samples ($p_4P_{200}t_{300}$, $p_{0.667}P_{200}t_{300}$, $p_4P_{280}t_{300}$, and $p_4P_{120}t_{300}$); however, due to the fact that the barrier properties depend on the cerium content and film thickness, the as-deposited films at $p_{1.333}P_{200}t_{300}$ and $p_4P_{40}t_{300}$ have a tendency to lose the properties against corrosion. For bare aluminum, it is clear that the value of R_p increased with the immersion time. Scully has stated that the electrochemical nature of the corrosion of totally immersed specimens that are susceptible to pit is usually determined by the diffusion of oxygen to cathodic sites; when this is so, the total weight loss in the specimens is then proportional to the area of the liquid surface [44]. In that case, the physical state of the product of a corrosion reaction can have a high effect upon its progress, while rust forms away from the active sites and has no direct effect; other products form flocculants or very hard precipitates, depending upon temperature, oxygen concentration, acidity, etc. Subsequently, pits are often covered with a membrane of product that severely restricts the access of oxygen and partially increase the total resistance. Such product is usually the hydroxide precipitation:

$$Al^{3+} + 3OH^- \rightarrow Al(OH)_3 \quad (3)$$

This classical behavior in aluminum alloys may explain the observed increase in the impedance values for bare aluminum and the poor performance for the Al–Ce films with low cerium contents ($p_{1.333}P_{200}t_{300}$ and $p_4P_{40}t_{300}$). Additionally, the differences in the impedance values and in the low-frequency tail with the immersion time for the other samples can also be correlated with the formation of some cerium compounds and its dissolution during the corrosion process.

$$Ce^{3+} + 3H_2O \rightarrow Ce(OH)_3 + H^+ \quad (4)$$

$$Ce^{3+} + 3Cl^- \rightarrow CeCl_3 \quad (5)$$

Furthermore, due to the fact that the shape of the EIS spectra was not modified with the sputtered Al–Ce coatings, it is clear that the films are only delaying pitting corrosion by inhibiting cathodic and/or anodic reactions and increasing the overall polarization resistance values, i.e. the good corrosion resistance obtained at some experimental conditions ($p_4P_{200}t_{300}$, $p_{0.667}P_{200}t_{300}$, $p_4P_{280}t_{300}$, and $p_4P_{120}t_{300}$) can be attributed to the coatings insulating the alloy matrix from the corrosion medium inhibiting the free diffusion of oxygen. Then, the observed electrochemical performance and XPS analyses match with the self-healing characteristics of cerium oxides (specially in the form of Ce^{4+}) observed in aggressive medium, which in our case increased as the Al/Ce ratio was increased.

3.3 Surface characterization and composition of the sputtered Al–Ce coatings on AA6061 aluminum alloy after electrochemical tests

The surface and corresponding XRD spectra of selected sputtered Al–Ce coatings and bare AA6061 aluminum alloy exposed to a 3.5 wt% NaCl solution after 21 days are shown in Fig. 8a–d.

The SEM micrographs for bare aluminum after 21 days of continuous immersion displayed the typical corrosion behaviour of these aluminum alloys in chloride solutions (Fig. 8a), where pits are nucleated all over the oxide film and likely to be discontinuous, causing hemispherical pits with different sizes [45]. At this time, it was observed that few highly deep pits occurred at the surface of bare aluminum. These samples began to present visible attack after 1 day; afterward, as time increased, the sample began to

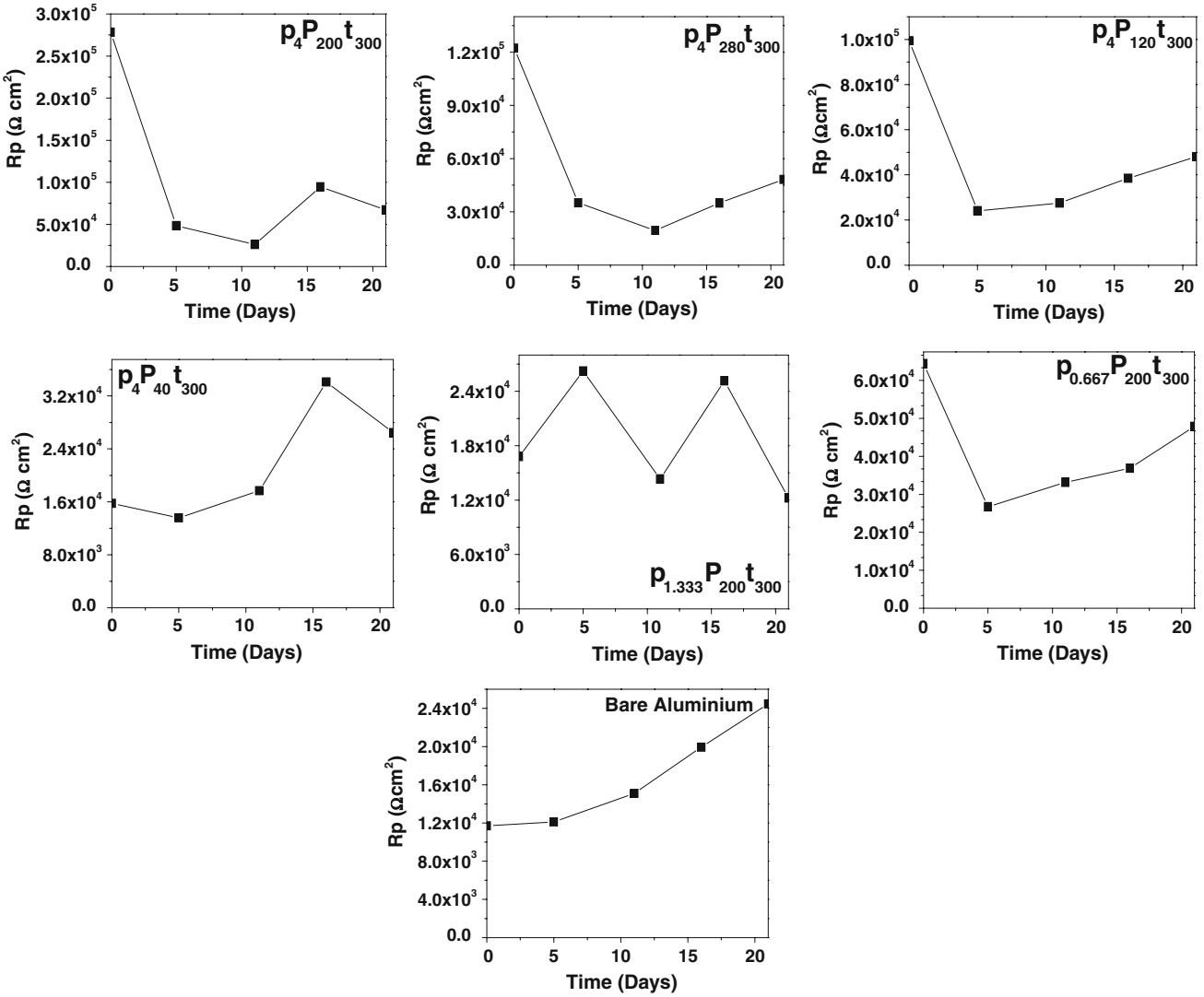

Fig. 7 Evolution of overall polarization resistance values with exposure time of sputtered Al–Ce coatings and bare AA6061 aluminum alloy in a 3.5 wt% NaCl aqueous solution

cover with a layer of white corrosion products on the surface, which were mainly composed of $Al(OH)_3$. Finally, at this time, the layer had a spongy texture, which when magnified revealed a deeply attacked structure. Also, it can be observed the formation of $AlCl_3$ on the substrate surface. Attack on aluminum alloys with similar morphology has been reported by other authors in this aggressive medium [21, 45]. On the other hand, the SEM micrographs of the selected sputtered Al–Ce coatings after 21 days in the 3.5 wt% NaCl solution are shown in Fig. 8b–d. The noticeable changes in the surface morphology of the as-deposited Al–Ce films highlight the importance of the Al/Ce ratio that can be reached depending on the deposition parameters. In the as-deposited films at $p_4P_{40}t_{300}$, hemispherical pits with different sizes grew through the surface of the samples; in fact, with the exposure time, these samples behaved as bare aluminum. Although the characteristic white corrosion product is not clearly visible in these aluminum alloys, in the vicinity of the pits, the corrosion products are composed by $Al(OH)_3$ and $AlCl_3$; in addition, the XRD measurements also detected alumina and metallic aluminum. The micrographs for the Al–Ce coatings at $p_4P_{200}t_{300}$ and $p_4P_{280}t_{300}$ showed that although with less thickness due to some dissolution of the film, the Al–Ce films were still on the substrate surface, diminishing the corrosion attack, even when at the $p_4P_{280}t_{300}$, the typical white corrosion products are clearly observed in the micrograph. In fact, the pits could begin to nucleate on the erosion areas of the surface of the Al–Ce films. The presence of $CeCl_3$, $Ce(OH)_3$ as well as some intermetallic compounds (overlapping with other aluminum products) detected by XRD measurements may confirm the assumption that the film remains on the substrate surface. The formation of pits on native-oxide-film-covered

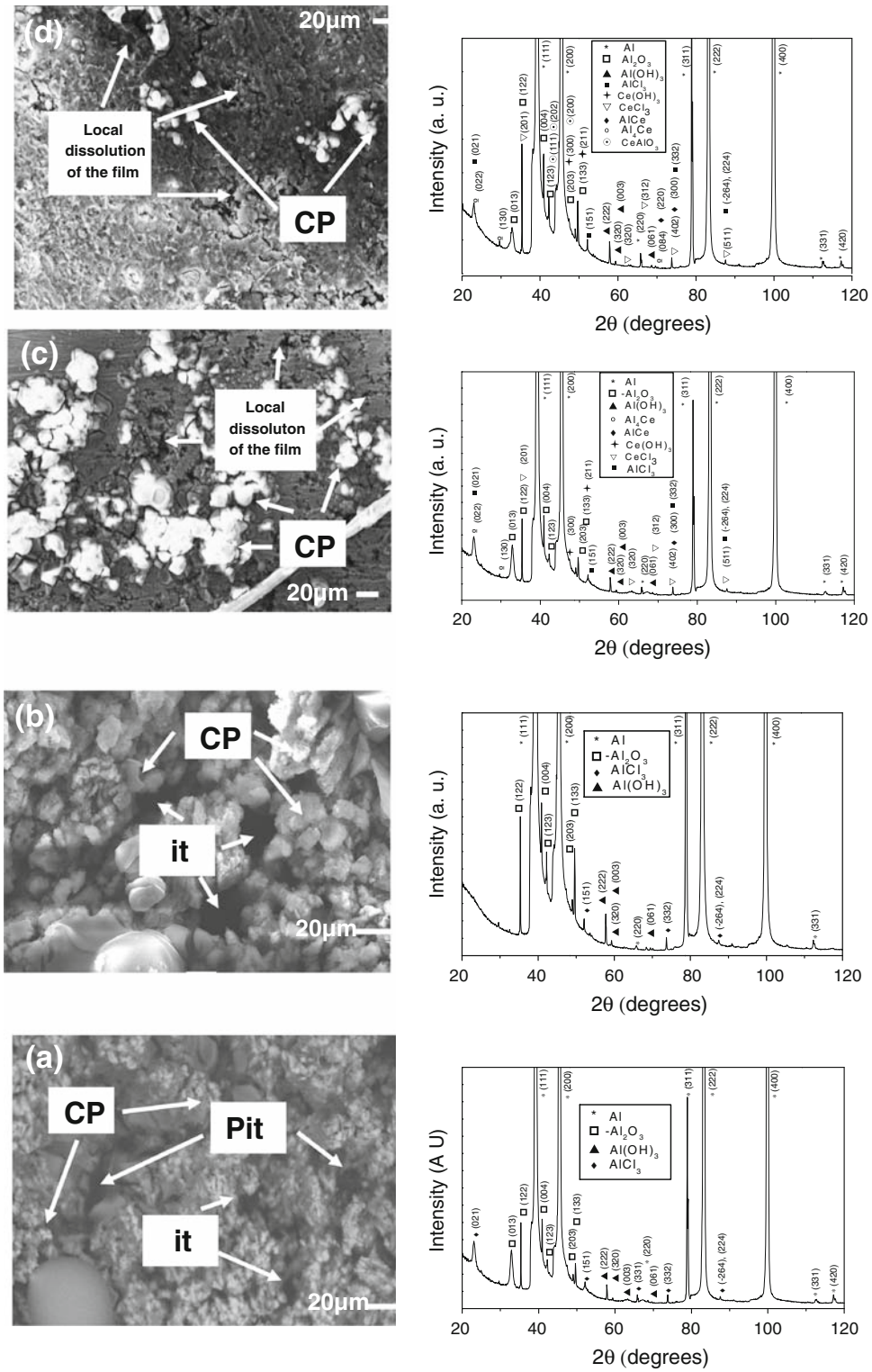

Fig. 8 SEM images and XRD measurements of **a** bare aluminum and sputtered Al–Ce coatings at **b** $p_{30}P_{40}t_{300}$, **c** $p_{30}P_{280}t_{300}$, and **d** $p_{30}P_{200}t_{300}$ after 21 days of exposure in a 3.5 wt% NaCl solution

aluminum has been previously reported [46–49] and it is well accepted that the incorporation of chloride ions into the oxide film on aluminum is a partial step for pitting corrosion. Ren and Zuo [47] stated that two main modes may control the initiation of the pit; either the absorbed Cl ions are transported through the oxide film by means of oxygen vacancies or Cl^- ions migrate to the film/aluminum boundary through the defects in the surface [50]. In such conditions, the formation of some soluble species such as $AlCl_3$ and $CeCl_3$ and their dissolution are possible, which may explain the dissolution of sputtered Al–Ce films after 21 days of immersion at $p_{0.667}P_{200}t_{300}$, $p_{1.333}P_{200}t_{300}$ and

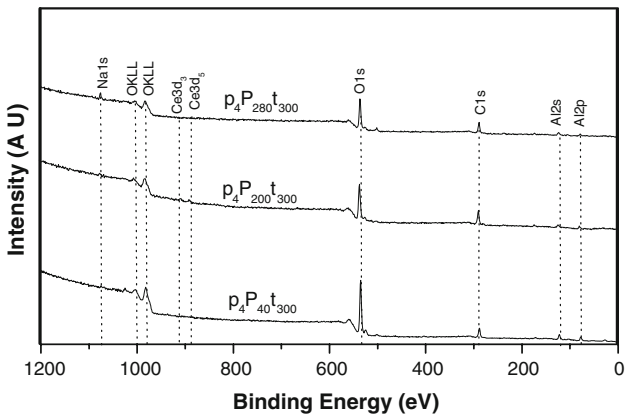

Fig. 9 XPS survey spectra of the Al–Ce coatings after the electrochemical test at different deposition parameters on AA6061 aluminum alloys

$p_4P_{40}t_{300}$ with low film thickness and Al/Ce ratio, and the formation of $CeCl_3$ compounds detected in the films at $p_4P_{200}t_{300}$ and $p_4P_{280}t_{300}$.

To confirm the previous results, the low-resolution XPS spectra of selected samples ($p_4P_{200}t_{300}$, $p_4P_{280}t_{300}$, $p_4P_{40}t_{300}$) after electrochemical tests are shown in Fig. 9. From the results shown in this figure, it can be seen that the surface composition contains mainly Na, O, Al and different amounts of Ce. C is again observed and its presence can be due to the accumulation of contaminants during the exposure to air [25, 26], whereas Cl^- is missing in the XPS spectra.

High-resolution Ce3d XPS spectra obtained on surface at $p_4P_{200}t_{300}$ sputtered Al–Ce films after electrochemical measurements displayed the presence of Ce^{3+} as well as Ce^{4+} (Fig. 10). The Ce3d spectra of these samples were similar to those obtained before the electrochemical test. Therefore, the spectra were curve-fitted to two peaks to obtain the individual contribution of the cerium oxide compounds (Ce_2O_3 and CeO_2). In contrast, in the as-deposited samples at $p_4P_{280}t_{300}$ and $p_4P_{40}t_{300}$ films, the Ce3d peaks were very noisy and very hard to be fitted and to separate the contribution of cerium compounds.

The high-resolution O1s spectra at different deposition parameters are shown in Fig. 11. From the XRD results, the O1s spectra in the samples at different deposition parameters were attributed to the Al–O group (531.5 eV), Ce–OH group (532 eV) [51] or Al–OH group (532 eV) and the Ce–O group (529.5 eV); and based in these groups the O1s was fitted in Fig. 11. While the $p_4P_{200}t_{300}$ and $p_4P_{280}t_{300}$ samples displayed the presence of Al–OH or Ce–OH, Al–O and Ce–O bonds, the $p_4P_{40}t_{300}$ samples only showed Al–OH, Al–O bonds, which confirmed the XRD

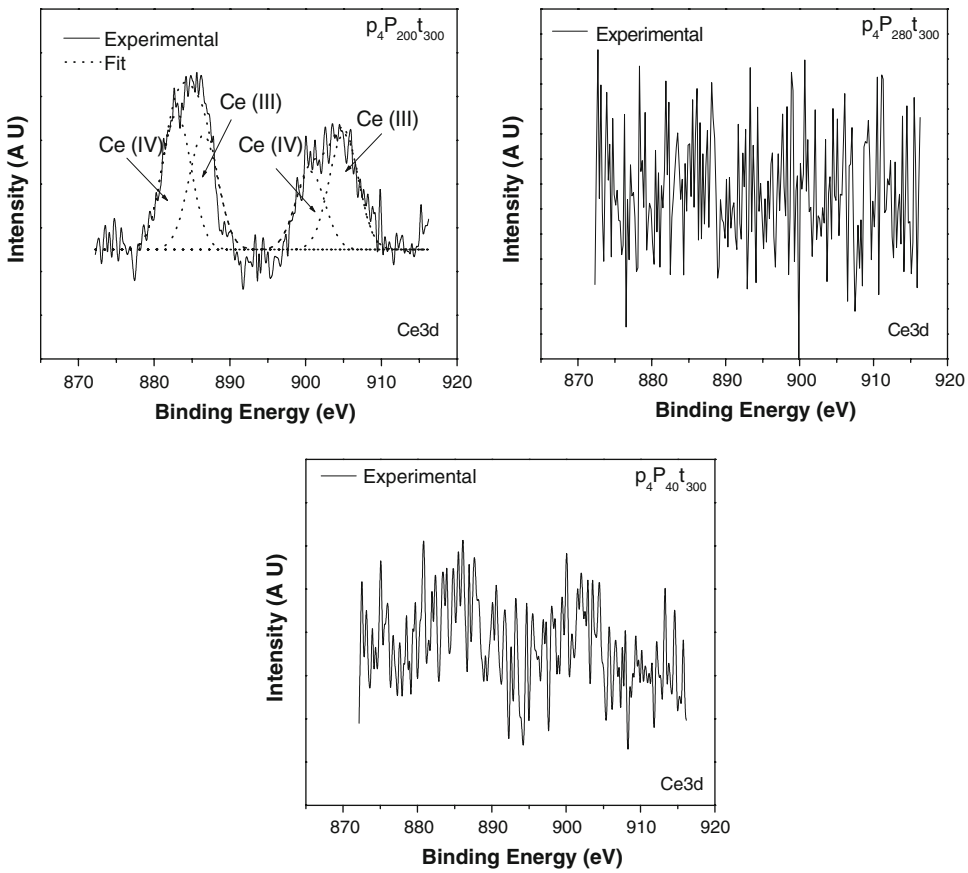

Fig. 10 High-resolution Ce3d XPS spectra obtained on the surface of selected sputtered Al–Ce films after electrochemical measurements

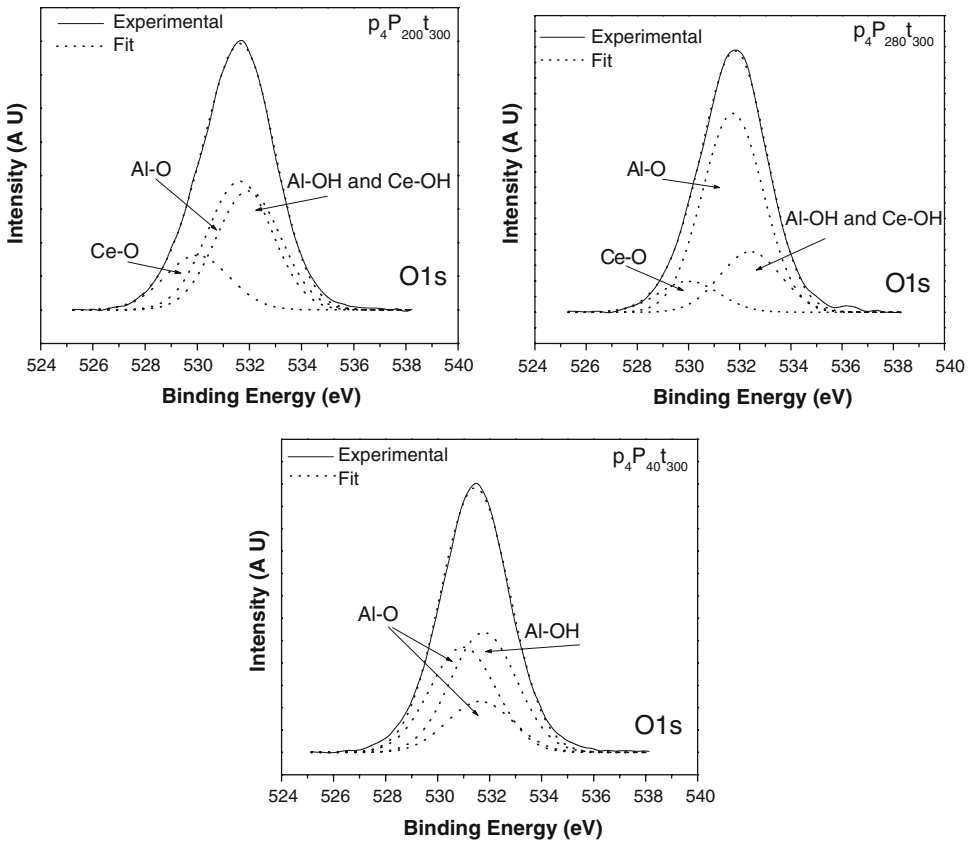

Fig. 11 High-resolution O1s XPS spectra obtained on the surface of selected sputtered Al–Ce films after electrochemical measurements

results. Then, Ce_2O_3, CeO_2, Al_2O_3, and Al in combination with an amount of corrosion products ($CeCl_3$, $AlCl_3$, $Ce(OH)_3$ and/or $Al(OH)_3$) and some intermetallic compounds detected by XRD measurements (Al_4Ce, AlCe, AlCeO) composed the film after 21 days of exposure at $p_4P_{200}t_{300}$ and $p_4P_{280}t_{300}$. On the other hand, Al_2O_3 and Al in combination with $Al(OH)_3$ and $AlCl_3$ were observed in the $p_4P_{40}t_{300}$ samples, which evidenced the dissolution of the films after this time. Finally, the atomic Ce^{3+}/Ce^{4+} ratio at $p_4P_{200}t_{300}$ is shown in Table 1. From this table, it can be observed that the Ce^{3+}/Ce^{4+} ratio at $p_4P_{200}t_{300}$ is very close before and after the electrochemical measurements, which may explain the good electrochemical performance after 21 days of continuous immersion.

4 Conclusions

The XPS and EIS techniques were used to interpret the electrochemical performance of sputtered Al–Ce coatings with the exposure time in a 3.5 wt% NaCl solution for 21 days. The XPS study corroborated that the Al–Ce films were initially deposited in the metallic form, and thereafter, the surface oxidation under the environmental conditions occurred, i.e., the sputtered coatings were mainly composed of Al, Ce and their intermetallic compounds, which were oxidized on the surface forming Ce_2O_3, CeO_2 and Al_2O_3; although the signals of intermetallic compounds such as Ce, $CeAlO_3$, Al_4Ce and Al_3Ce were missing in the XPS spectra, which was probably due to the overlapping with Ce^{4+} bond signals. The important variation in the R_p values indicated a clearly correlation with the film thickness and Al/Ce ratio; an increase in the Al/Ce ratio reduced the activity of the AA6061 aluminum alloy with the immersion time in the aggressive medium; however, such an increase can be limited by the gas rarefication caused by a higher amount of reactive cerium atoms in the plasma and the sputter yield of Al and Ce or both. The changes in impedance values and in the tail at low frequencies are clearly related to the dissolution of the sputtered Al–Ce films and the diffusive controlled process due to the evolution of the corrosion process. The EIS results support that the films are only delaying pitting corrosion by inhibiting cathodic and/or anodic reactions and increasing the overall polarization resistance values. After electrochemical tests, the SEM images indicated that the Al–Ce films with the lowest Al/Ce ratios ($p_4P_{40}t_{300}$, $p_{0.667}P_{200}t_{300}$, $p_{1.333}P_{200}t_{300}$) lost their electrochemical properties and behaved as bare aluminum; as for the Al–Ce samples at $p_4P_{120}t_{300}$, $p_4P_{200}t_{300}$, $p_4P_{280}t_{300}$, the presence of $CeCl_3$ and

$Ce(OH)_3$ detected by XRD measurements confirmed the SEM observations, which indicated that the film remained on the substrate surface. Finally, from the XPS results, it could be seen that the Ce^{3+}/Ce^{4+} ratio at $p_4P_{200}t_{300}$ was very close before and after the electrochemical measurements, which matched with the good electrochemical performance showed after 21 days of continuous immersion due to the self-healing characteristics of cerium oxides.

Acknowledgments This study has been financially supported by CONACYT (project number 61354), IPN (projects number SIP-2009-0561, 2009-0499) and SNI. The authors would like to thank Mr. Javier Zapata Torres for his technical support.

References

1. Szklarska-Smialowska Z (1999) Corros Sci 41:1743
2. Sun X, Zhou X, Thompson GE, Skeldon P, Shimizu K, Furneaux RC, Scamans G (1998) Sixth international conference on aluminium alloys vol 3, p 1571
3. Davis JR (ed) (1999) Corrosion of aluminium and aluminium alloys. ASM International, Materials Park
4. Habazaki H, Shimizu K, Skeldon P, Thompson GE, Wood GC, Zhou X (1997) Corros Sci 39:731
5. Mujibur Rahman ABM, Kumar S, Gerson AR (2008) Corros Sci 50:1267
6. Voevodin N, Jeffcoate C, Simon L, Khobaib M, Donley M (2001) Surf Coat Technol 140:29
7. Sander LS, Musingo EM, Neill WJ (1990) US Patent 4,921,552
8. Das N (1992) US Patent 5,139,586
9. Miller RN (1994) US Patent 5,356,492
10. Tomlinson CE (1995) US Patent 5,380,374
11. Hinton BRW, Arnott DR, Ryan NE (1986) Mater Forum 9:162
12. Mansfeld F, Lin S, Kim S, Shih H (1989) Electrochim Acta 34:1123
13. Domínguez-Crespo MA, Rodil SE, Torres-Huerta AM, Ramírez-Meneses E, Suárez-Velázquez G (2009) Surf Coat Technol 204:571
14. Sheng HW, Liu HZ, Cheng YQ, Wen J, Lee PL, Luo WK, Shastri SD, Ma E (2007) Nat Mater 6:192
15. Mazurkiewicz B, Piotrowski A (1983) Corros Sci 23:697
16. Blanc C, Lavelle B, Mankowski G (1996) Mater Sci Forum 217:1559
17. Vyazovikina NV (1999) Protect Met 35:448
18. Okamoto G, Shibata T (1978) In: Frankenthal RP, Kruger J (eds) Passivity of metals, Corrosion monograph series, The Electrochemical Society, Pennington, NJ
19. Blanc C, Mankowski G (1997) Corros Sci 39:949
20. Blanc C, Lavelle B, Mankowski G (1997) Corros Sci 39:495
21. Aballe A, Bethencourt M, Botana FJ, Cano MJ, Marcos M (2001) Corros Sci 43:1657
22. Bethencourt M, Botana FJ, Calvino JJ, Marcos M, Rodriguez MA (1998) Mater Sci Forum 289–292:567
23. Ambat R, Dwarakadasa ES (1994) J Appl Electrochem 24:911
24. Wallinder D, Pan J, Leygraf C, Delblanc-Bauer A (1999) Corros Sci 41:275
25. Yu X, Li G (2004) J Alloys Compd 264:193
26. Pan M, Meng GY, Xin HW, Chen CS, Peng DK, Lin YS (1998) Thin Solid Films 324:89
27. Pardo A, Merino MC, Arrabal R, Viejo F, Munoz JA (2007) Appl Surf Sci 253:3334
28. Teterin YA, Teterin AY, Lebedev AM, Utkin IO (1998) J Electron Spectrosc Relat Phenom 88–91:275
29. Arnott DR, Ryan NE, Hinton BRW, Sexton BA, Hughes AE (1985) Appl Surf Sci 22–23:236
30. Yu X, Li G (2004) J Alloys Compd 364:193
31. Domínguez-Crespo MA, Torres-Huerta AM, Rodil SE, Ramírez-Meneses E, Suárez-Velázquez G, Hernández-Pérez MA (2009) Electrochim Acta 55:498
32. Goeminne G, Terryn H, Vereecken J (1998) Electrochim Acta 43:1829
33. Campestrini P, Westing V, Wit JH (2001) Electrochim Acta 46:2631
34. Goeminne G, Terryn H, Vereecken J (1995) Electrochim Acta 40:479
35. Moutarlier V, Gigandet MP, Normand, Pagetti BJ (2005) Corros Sci 47:937
36. Palomino LEM, Aoki IV, de Melo HG (2006) Electrochim Acta 51:5943
37. López DA, Simison SN, de Sánchez SR (2005) Corros Sci 47:735
38. Bilkova K, Hackerman N, Bartos M (2002) Proceedings of the NACE corrosion, paper no. 2284, Denver, CO
39. Scully JR (1993) Electrochemical impedance: analysis and interpretation. ASTM STP 1188, p 26
40. Bessone JB, Salinas DR, Mayer CE, Ebert M, Lorenz WJ (1992) Electrochim Acta 37:2283
41. Xingwen Y, Chunan C, Zhiming Y, Derui Z, Zhongda Y (2001) Corros Sci 43:1283
42. Hughes AE, Gorman JD, Patterson PJK (1996) Corros Sci 38:1957
43. Gorman JD, Jhonson ST, Joghnston PN, Patterson PJK, Hughes AE (1996) Corros Sci 38:1977
44. Scully JC (1990) The fundaments of corrosion, 3rd edn. Pergamon Press, Oxford
45. Zaid B, Saidi D, Benzaid A, Hadji S (2008) Corros Sci 50:1841
46. Meng G, Wei L, Zhang T, Shao Y, Wang F, Dong C, Li X (2009) Corros Sci 51:2151
47. Ren J, Zuo Y (2005) Surf Coat Technol 191:311
48. Yu SY, O'Grady WE, Ramaker DE, Natishan PM (2000) J Electrochem Soc 147:2952
49. Pyun SI, Lee WJ (2001) Corros Sci 43:153
50. Moutarlier V, Gigandet MP, Pagetti J (2003) Appl Surf Sci 206:237
51. Zhang H, Zuo Y (2008) Appl Surf Sci 254:4930